Inorganica Chimica Acta 384 (2012) 54–61

Contents lists available at SciVerse ScienceDirect

Inorganica Chimica Acta

journal homepage: www.elsevier.com/locate/ica

Synthesis, structures, and urease inhibitory activities of oxovanadium(V) complexes with Schiff bases

Zhong-Lu You [a,*], Da-Hua Shi [b], Ji-Cai Zhang [a], Yu-Ping Ma [a], Che Wang [a], Kun Li [a]

[a] Department of Chemistry and Chemical Engineering, Liaoning Normal University, Dalian 116029, PR China
[b] School of Chemical Engineering, Huaihai Institute of Technology, Lianyungang 222005, PR China

ARTICLE INFO

Article history:
Received 30 May 2011
Received in revised form 9 November 2011
Accepted 12 November 2011
Available online 6 December 2011

Keywords:
Schiff base
Oxovanadium complex
Crystal structure
Urease inhibition

ABSTRACT

A series of oxovanadium(V) complexes, $[VO_2L^1]_2$ (**1**), $[VO_2L^2]_2$ (**2**), $[VO_2L^3]_2$ (**3**), $[VO_2L^4]_2$ (**4**), $[VO(OCH_3)L^5]$ (**5**), and $[VO(OCH_3)(HOCH_3)L^6]$ (**6**) (HL^1 = 2-ethoxy-6-{[2-(2-hydroxyethylamino)ethylimino]methyl}phenol, HL^2 = 4-chloro-2-{[2-(2-hydroxyethylamino)ethylimino]methyl}phenol, HL^3 = 2-methoxy-6-[(2-methylaminoethylimino)methyl]phenol, HL^4 = 4-chloro-2-[(2-methylaminoethylimino)methyl]phenol, HL^5 = *N*′-(2-hydroxy-3-ethoxybenzylidene)-3-hydroxy-2-naphthohydrazide, and HL^6 = *N*′-(2-hydroxy-5-chlorobenzylidene)-3-hydroxy-2-naphthohydrazide), have been prepared and structurally characterized by physico-chemical methods and X-ray diffraction. The inhibition rates (%) with the concentration of 100 μM for the complexes on *Helicobacter pylori* urease are 18.96 ± 0.44 (**1**), 33.01 ± 1.80 (**2**), 35.83 ± 0.78 (**3**), 48.09 ± 1.23 (**4**), 45.91 ± 2.09 (**5**), and 90.72 ± 1.91 (**6**). The relationship between the structures and urease inhibitory activities indicates that the chloro-substituted complexes have stronger activity than the alkoxy-substituted complexes. It is notable that one of the chloro-substituted complexes has very strong urease inhibitory activity, with IC_{50} value of 17.35 ± 1.01 μM, which is much lower than that of the acetohydroxamic acid coassayed as a standard urease inhibitor. The kinetic studies reveal that the complex is a mixed-competitive inhibitor of urease. The molecular docking study of the complexes with the *Helicobacter pylori* urease was performed.

1. Introduction

Urease is a nickel-containing metalloenzyme that catalyzes the hydrolysis of urea to form ammonia and carbamate [1,2]. The resulting carbamate spontaneously decomposes to yield a second molecule of ammonia and carbon dioxide. High concentration of ammonia arising from these reactions, as well as the accompanying pH elevation, have important negative implication in medicine and agriculture [3–6]. Control of the activity of urease through the use of inhibitors could counteract these negative effects. In recent years, urease inhibitors have played an important role in the treatment of the infections caused by urease producing bacteria [7]. Inhibitors of urease can be broadly classified into two fields: (1) organic compounds, such as acetohydroxamic acid, humic acid, and 1,4-benzoquinone [8–10]; (2) heavy metal ions, such as Cu^{2+}, Zn^{2+}, Pd^{2+}, and Cd^{2+} [11,12]. Considering the metal complexes are a kind of versatile enzyme inhibitors [13], we have recently reported the properties of a number of complexes with Schiff bases [14–16]. The results show that the Schiff base copper(II) complexes have potential urease inhibitory activities. Vanadium complexes have been widely investigated in biological chemistry, especially for their insulin-enhancing activities [17–19]. After searching the literature, we find that the vanadium(IV) complexes also possess interesting urease inhibitory activity [20]. As an extensive study on the oxovanadium complexes and their urease inhibitory activity, in this paper, a series of new oxovanadium(V) complexes, $[VO_2L^1]_2$ (**1**), $[VO_2L^2]_2$ (**2**), $[VO_2L^3]_2$ (**3**), $[VO_2L^4]_2$ (**4**), $[VO(OCH_3)L^5]$ (**5**), and $[VO(OCH_3)(HOCH_3)L^6]$ (**6**) (HL^1 = 2-ethoxy-6-{[2-(2-hydroxyethylamino)ethylimino]methyl}phenol, HL^2 = 4-chloro-2-{[2-(2-hydroxyethylamino)ethylimino]methyl}phenol, H_2L^3 = 2-methoxy-6-[(2-methylaminoethylimino)methyl]phenol, H_2L^4 = 4-chloro-2-[(2-methylaminoethylimino)methyl]phenol, HL^5 = *N*′-(2-hydroxy-3-ethoxybenzylidene)-3-hydroxy-2-naphthohydrazide, HL^6 = *N*′-(2-hydroxy-5-chlorobenzylidene)-3-hydroxy-2-naphthohydrazide; Scheme 1) were synthesized and structurally characterized. The urease inhibitory activity of the complexes was investigated both from the experimental and from the docking analysis using the AutoDock 4.0 program [21].

2. Experimental

2.1. General remarks and physical measurements

Reagents and solvents were purchased from commercial suppliers and were used without further purification. Protease inhibitor

* Corresponding author. Tel.: +86 411 84216387.
E-mail address: youzhonglu@yahoo.com.cn (Z.-L. You).

0020-1693/$ - see front matter © 2011 Elsevier B.V. All rights reserved.
doi:10.1016/j.ica.2011.11.039

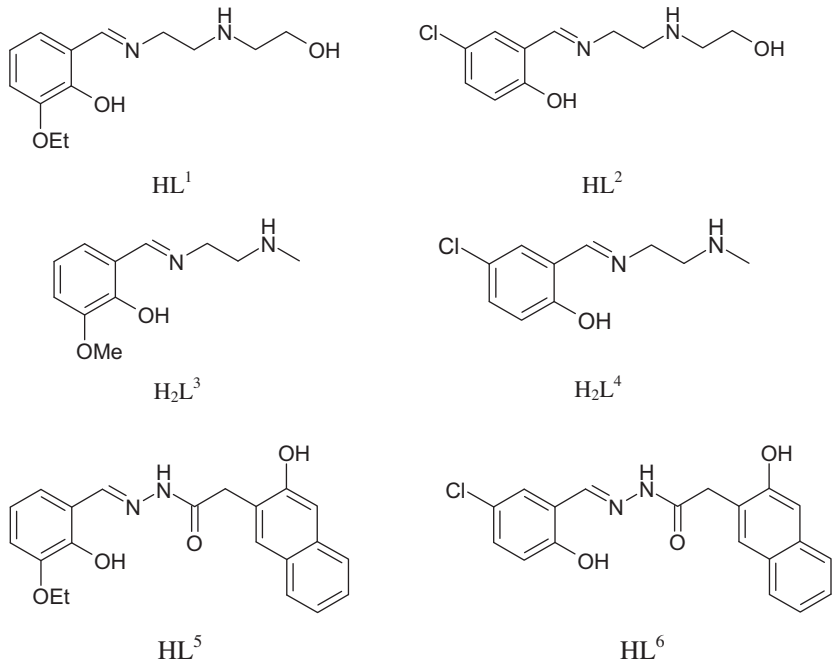

Scheme 1. The Schiff bases.

(Complete mini EDTA-free) was purchased from Roche Diagnostics GmbH (Mannhein, Germany) and Brucella broth was from [Becton–Dickinson] (Cockeysville, MD). Horse serum was obtained from Hyclone (Utah, America). Elemental analyses were performed on a Perkin-Elmer 240C elemental analyzer. The IR spectra were recorded on a Jasco FT/IR-4000 spectrometer as KBr pellets in the 4000–200 cm^{-1} region. Molar conductance was measured with a Shanghai DDS-11A conductometer. X-ray diffraction was carried out on a Bruker SMART 1000 CCD area diffractometer. UV–vis spectra were recorded on a Perkin-Elmer Lambda 9 instrument. The EPR spectra of the complexes were measured using a Bruker EMX Micro Premium X spectrometer.

2.2. Synthesis of the Schiff bases

To a methanolic solution (50 mL) of substituted salicylaldehyde (2.0 mmol) a methanolic solution (30 mL) of primary amine (2.0 mmol) was added with continuous stirring. The mixture was stirred for 30 min at room temperature to give yellow solution. The solvent was evaporated to give yellow gummy product of the Schiff base, which was washed with methanol and dried in air. Yields: 83–87%. *Anal.* Calc. for $C_{13}H_{20}N_2O_3$ (HL^1): C, 61.9; H, 8.0; N, 11.1. Found: C, 61.7; H, 8.1; N, 11.3%. *Anal.* Calc. for $C_{11}H_{15}ClN_2O_2$ (HL^2): C, 54.4; H, 6.2; N, 11.5. Found: C, 54.7; H, 6.3; N, 11.5%. *Anal.* Calc. for $C_{11}H_{16}N_2O_2$ (HL^3): C, 63.4; H, 7.7; N, 13.4. Found: C, 63.6; H, 7.7; N, 13.2%. *Anal.* Calc. for $C_{10}H_{13}ClN_2O$ (HL^4): C, 56.5; H, 6.2; N, 13.2. Found: C, 56.1; H, 6.3; N, 13.3%. *Anal.* Calc. for $C_{21}H_{20}N_2O_4$ (HL^5): C, 69.2; H, 5.5; N, 7.7. Found: C, 69.5; H, 5.5; N, 7.6%. *Anal.* Calc. for $C_{19}H_{15}ClN_2O_3$ (HL^6): C, 64.3; H, 4.3; N, 7.9. Found: C, 64.6; H, 4.4; N, 7.6%.

2.3. Synthesis of the complexes

A methanolic solution (20 mL) of the Schiff base (0.5 mmol) was added with stirring to a methanolic solution (20 mL) of $VO(acac)_2$ (0.5 mmol, 0.133 g). The mixtures were stirred at room temperature for 30 min to give solutions with color from yellow to deep brown. X-ray quality single crystals were formed by slow evaporation of the solutions in air after a few days.

2.3.1. Bis(μ_2-oxo)bis(2-ethoxy-6-{[2-(2-hydroxyethylamino)ethylimino]methyl}phenolato)dioxodivanadium(V) (**1**)

Yellow single crystals. Yield: 62%. *Anal.* Calc. for $C_{26}H_{38}N_4O_{10}V_2$: C, 46.7; H, 5.7; N, 8.4. Found: C, 46.4; H, 5.9; N, 8.2%. IR data: 3371 (m), 3202 (w), 1640 (s), 1598 (m), 1557 (w), 1468 (s), 1448 (s), 1418 (w), 1392 (m), 1292 (s), 1253 (s), 1223 (m), 1174 (w), 1112 (w), 1079 (m), 1044 (m), 996 (w), 914 (s), 856 (s), 785 (w), 748 (m), 636 (w), 614 (w), 477 (w), 441 (w), 373 (w), 349 (w), 326 (w). UV–vis spectra data in DMSO [nm (ε, $M^{-1}\,cm^{-1}$)]: 256 (1.4×10^4), 370 (3.4×10^3), 563 (172).

2.3.2. Bis(μ_2-oxo)bis(4-chloro-2-{[2-(2-hydroxyethylamino)ethylimino]methyl}phenolato)dioxodivanadium(V) (**2**)

Yellow single crystals. Yield: 67%. *Anal.* Calc. for $C_{22}H_{28}Cl_2N_4O_8V_2$: C, 40.7; H, 4.3; N, 8.6. Found: C, 41.0; H, 4.5; N, 8.5%. IR data: 3464 (m), 3211 (w), 1638 (s), 1593 (w), 1539 (m), 1465 (s), 1383 (s), 1335 (w), 1292 (s), 1201 (w), 1182 (m), 1133 (w), 1093 (w), 1061 (m), 1020 (m), 970 (w), 921 (m), 886 (m), 841 (s), 707 (m), 660 (w), 549 (w), 526 (w), 454 (w), 426 (w), 339 (w), 326 (w). UV–vis spectra data in DMSO [nm (ε, $M^{-1}\,cm^{-1}$)]: 253 (1.4×10^4), 372 (3.2×10^3), 558 (183).

2.3.3. Bis(μ_2-oxo)bis(2-methoxy-6-[(2-methylaminoethylimino)methyl]phenolato)dioxodivanadium(V) (**3**)

Orange single crystals. Yield: 72%. *Anal.* Calc. for $C_{22}H_{30}N_4O_8V_2$: C, 45.5; H, 5.2; N, 9.7. Found: C, 45.3; H, 5.4; N, 9.6%. IR data: 3235 (w), 1635 (s), 1598 (m), 1557 (w), 1471 (s), 1456 (s), 1397 (m), 1312 (s), 1251 (s), 1226 (s), 1173 (w), 1157 (w), 1085 (m), 1047 (w), 1024 (w), 969 (w), 929 (s), 837 (s), 783 (w), 744 (m), 635 (w), 610 (w), 573 (w), 472 (w), 437 (w), 401 (w), 353 (w). UV–vis spectra data in DMSO [nm (ε, $M^{-1}\,cm^{-1}$)]: 251 (1.3×10^4), 367 (3.2×10^3), 561 (167).

*2.3.4. Bis(μ_2-oxo)bis(4-chloro-2-[(2-methylaminoethylimino)methyl] phenolato)dioxodivanadium(V) (**4**)*

Orange single crystals. Yield: 54%. *Anal.* Calc. for $C_{20}H_{24}Cl_2N_4O_6V_2$: C, 40.8; H, 4.1; N, 9.5. Found: C, 40.5; H, 4.2; N, 9.5%. IR data: 3247 (w), 1649 (s), 1594 (w), 1538 (m), 1463 (s), 1421 (w), 1376 (m), 1302 (s), 1185 (m), 1090 (m), 1058 (w), 1012 (w), 933 (s), 854 (s), 806 (m), 708 (m), 660 (w), 545 (m), 466 (w), 453 (w), 402 (w), 364 (w), 318 (w). UV–vis spectra data in DMSO [nm (ε, M^{-1} cm^{-1})]: 258 (1.4×10^4), 389 (3.5×10^3), 572 (186).

*2.3.5. Methoxy(N′-(2-hydroxy-3-ethoxybenzylidene)-3-hydroxy-2-naphthohydrazonato)oxovanadium(V) (**5**)*

Brown single crystals. Yield: 65%. *Anal.* Calc. for $C_{21}H_{19}N_2O_6V$: C, 56.5; H, 4.3; N, 6.3. Found: C, 56.2; H, 4.5; N, 6.2%. IR data: 1638 (s), 1600 (s), 1575 (w), 1557 (m), 1525 (m), 1470 (m), 1445 (m), 1342 (w), 1305 (w), 1273 (m), 1251 (s), 1183 (w), 1145 (w), 1111 (m), 1072 (s), 990 (s), 891 (w), 861 (w), 763 (m), 738 (m), 633 (m), 536 (w), 478 (w), 361 (w), 337 (w). UV–vis spectra data in DMSO [nm (ε, M^{-1} cm^{-1})]: 235 (3.5×10^4), 260 (2.3×10^4), 335 (1.9×10^4).

*2.3.6. Methanolmethoxy(N′-(2-hydroxy-5-chlorobenzylidene)-3-hydroxy-2-naphthohydrazonato)oxovanadium(V) (**6**)*

Brown single crystals. Yield: 77%. *Anal.* Calc. for $C_{20}H_{18}ClN_2O_6V$: C, 51.2; H, 3.9; N, 6.0. Found: C, 51.4; H, 3.8; N, 6.1%. IR data: 3429 (m), 1641 (s), 1605 (m), 1577 (w), 1541 (s), 1521 (s), 1466 (m), 1386 (w), 1364 (m), 1341 (m), 1309 (m), 1279 (m), 1243 (w), 1220 (m), 1195 (w), 1148 (w), 1060 (s), 1027 (w), 985 (m), 873 (w), 823 (m), 747 (s), 716 (w), 669 (w), 632 (m), 572 (w), 507 (w), 482 (w), 343 (w). UV–vis spectra data in DMSO [nm (ε, M^{-1} cm^{-1})]: 230 (1.9×10^4), 267 (2.1×10^4), 327 (2.2×10^4).

2.4. X-ray crystallography

Diffraction intensities for the complexes were collected at 298(2) K using a Bruker SMART 1000 CCD area diffractometer with MoKα radiation (λ = 0.71073 Å). The collected data were reduced using the SAINT program [22], and multi-scan absorption correction was performed using the SADABS program [23]. The structures were solved by direct method and refined against F^2 by full-matrix least-squares method using the SHELXTL package [24]. All non-hydrogen atoms were refined anisotropically. The amino H atoms in the complexes **1**–**4**, and the methanol H atom in the complex **6** were located from difference Fourier maps and refined isotropically, with N–H and O–H distances restrained to 0.90(1) and 0.85(1) Å, and with U_{iso}(H) set to 0.08 $Å^2$. The remaining H atoms in the complexes were placed in calculated positions and constrained to ride on their parent atoms. The O3 atom in complex **1** is disordered over two sites, with occupancies of 0.778(2) and 0.222(2). The crystallographic data for the complexes are summarized in Tables 1 and 2. Selected bond lengths and angles are listed in Table 3.

2.5. Measurement of urease inhibitory activity

Helicobacter pylori (ATCC 43504; American Type Culture Collection, Manassas, VA) was grown in Brucella broth supplemented with 10% heat-inactivated horse serum for 24 h at 37 °C under microaerobic condition (5% O_2, 10% CO_2, and 85% N_2). The method of the preparation of *H. pylori* urease by Mao [25] was followed. Briefly, broth cultures (50 mL, 2.0×10^8 CFU mL^{-1}) were centrifuged (5000*g*, 4 °C) to collect the bacteria, and after washing twice with phosphate-buffered saline (pH 7.4), the *H. pylori* precipitation was stored at −80 °C. While the *H. pylori* was returned to room temperature, and mixed with 3 mL of distilled water and protease inhibitors, sonication was performed for 60 s. Following centrifugation (15 000*g*, 4 °C), the supernatant was desalted through SephadexG-25 column (PD-10 columns, Amersham Pharmacia Biotech, Uppsala, Sweden). The resultant crude urease solution was added to an equal volume of glycerol and stored at 4 °C until use in the experiment. The mixture, containing 25 μL of the *H. pylori* urease and 25 μL of the test compound, was pre-incubated for 3 h at room temperature in a 96-well assay plate. Urease activity was determined by measuring ammonia production using the indophenol method as described by Weatherburn [26].

2.6. Kinetic studies

Enzyme activities were determined at room temperature using four concentrations of substrate (50, 100, 200, and 300 μM) in the

Table 1
Crystallographic and experimental data for the complexes **1**, **2**, and **3**.

Complex	**1**	**2**	**3**
Formula	$C_{26}H_{38}N_4O_{10}V_2$	$C_{22}H_{28}Cl_2N_4O_8V_2$	$C_{22}H_{30}N_4O_8V_2$
Formula weight	668.5	649.3	580.4
T (K)	298(2)	298(2)	298(2)
Crystal shape/color	block/orange	block/orange	block/yellow
Crystal size (mm^3)	0.23 × 0.21 × 0.20	0.27 × 0.23 × 0.22	0.30 × 0.30 × 0.23
Crystal system	monoclinic	monoclinic	monoclinic
Space group	$P2_1/n$	$P2_1/c$	$P2_1/c$
a (Å)	9.840(2)	7.239(2)	7.634(2)
b (Å)	6.751(1)	15.415(4)	20.341(3)
c (Å)	22.081(3)	11.744(3)	8.566(2)
β (°)	94.790(2)	99.532(2)	109.958(2)
V ($Å^3$)	1461.7(4)	1292.4(6)	1250.2(5)
Z	2	2	2
D_{calc} (g cm^{-3})	1.519	1.668	1.542
μ (MoKα) (mm^{-1})	0.701	0.985	0.801
F(000)	696	664	600
Data collected	3167	2805	1879
Unique data ($I \geqslant 2\sigma(I)$)	1876	2421	1382
Minimum and maximum transmission	0.855 and 0.873	0.777 and 0.812	0.795 and 0.837
Parameters	206	176	169
Restraints	9	1	1
Goodness-of-fit on F^2	0.997	1.052	1.036
R_1, wR_2 [$I \geqslant 2\sigma$ (I)][a]	0.0584, 0.1021	0.0302, 0.0763	0.0398, 0.0878
R_1, wR_2 (all data)[a]	0.1157, 0.1221	0.0361, 0.0792	0.0602, 0.0996
Large difference on peak and hole (e $Å^{-3}$)	0.300 and −0.460	0.333 and −0.333	0.309 and −0.265

[a] $R_1 = F_o - F_c/F_o, wR_2 = [\sum w(F_o^2 - F_c^2)/\sum w(F_o^2)^2]^{1/2}$.

Table 2
Crystallographic and experimental data for the complexes **4**, **5**, and **6**.

Complex	**4**	**5**	**6**
Formula	$C_{20}H_{24}Cl_2N_4O_6V_2$	$C_{21}H_{19}N_2O_6V$	$C_{20}H_{18}ClN_2O_6V$
Formula weight	589.2	446.3	468.7
T (K)	298(2)	298(2)	298(2)
Crystal shape/color	block/yellow	block/brown	block/brown
Crystal size (mm^3)	0.18 × 0.17 × 0.16	0.30 × 0.27 × 0.27	0.17 × 0.13 × 0.12
Crystal system	monoclinic	monoclinic	monoclinic
Space group	$P2_1/c$	$P2_1/c$	$P2_1/n$
a (Å)	6.803(1)	16.438(2)	13.445(2)
b (Å)	11.515(2)	6.325(1)	6.802(2)
c (Å)	15.137(3)	18.971(3)	22.505(3)
β (°)	97.144(2)	96.492(2)	102.216(3)
V ($Å^3$)	1176.6(3)	1960.0(6)	2011.5(7)
Z	2	4	4
D_{calc} ($g\,cm^{-3}$)	1.663	1.513	1.548
μ (Mo Kα) (mm^{-1})	1.066	0.548	0.667
F(000)	600	920	960
Data collected	2545	4166	4389
Unique data ($I \geqslant 2\sigma(I)$)	2316	3134	2116
Minimum and maximum transmission	0.831 and 0.848	0.853 and 0.866	0.895 and 0.924
Parameters	158	274	277
Restraints	1	0	1
Goodness-of-fit on F^2	1.051	1.047	0.990
R_1, wR_2 [$I \geqslant 2\sigma(I)$][a]	0.0269, 0.0732	0.0426, 0.1041	0.0660, 0.1149
R_1, wR_2 (all data)[a]	0.0301, 0.0753	0.0619, 0.1145	0.1611, 0.1454
Large difference on peak and hole (e $Å^{-3}$)	0.255 and −0.300	0.398 and −0.438	0.304 and −0.370

[a] $R_1 = F_o - F_c/F_o, wR_2 = [\sum w(F_o^2 - F_c^2)/\sum w(F_o^2)^2]^{1/2}$.

presence or absence of three concentrations of **6** (10, 20, and 40 μM). Then data were plotted by the method of Lineweaver–Burk to reveal the mechanism of inhibition. Replots of the slopes versus the inhibitor concentrations gave estimates of K_i, the dissociation constant for **6** binding to urease.

2.7. Docking study

Molecular docking study of the complexes into the 3D X-ray structure of the *H. pylori* urease (entry 1E9Y in the Protein Data Bank) was carried out by using the AutoDock 4.0 software as implemented through the graphical user interface AutoDockTools (ADT 1.5.2).

The graphical user interface AutoDockTools was employed to setup the enzymes: all hydrogens were added, Gasteiger charges were calculated and non-polar hydrogens were merged to carbon atoms. The Ni initial parameters are set as r = 1.170 Å, q = +2.0, and van der Waals well depth of 0.100 kcal/mol [27]. The 3D structures of the ligand molecules were saved in Mol2 format with the aid of the program Mercury. The partial charges of Mol2 file were further modified by using the ADT package so that the charges of the non-polar hydrogen atoms assigned to the atoms to which the hydrogen is attached. The resulting files were saved as pdbqt format.

The AutoDockTools was used to generate the docking input files. In all docking a grid box size of 90 × 90 × 90 points in x, y, and z directions was built, the maps were centered on the original ligand molecule in the catalytic site of the protein. A grid spacing of 0.375 Å and a distances-dependent function of the dielectric constant were used for the calculation of the energetic map. One hundred runs were generated by using Lamarckian genetic algorithm searches. Default settings were used with an initial population of 50 randomly placed individuals, a maximum number of 2.5×10^6 energy evaluations, and a maximum number of 2.7×10^4 generations. A mutation rate of 0.02 and a crossover rate of 0.8 were chosen. The results of the most favorable free energy of binding were selected as the resultant complex structures.

3. Results and discussion

The Schiff bases were synthesized by the reaction of equimolar quantities of chloro- or alkoxy-substituted salicylaldehydes with primary amines or hydrazones in methanol. All the complexes were synthesized by the reaction of the methanol solution of the Schiff bases with $VO(acac)_2$. The compounds have been characterized by elemental analysis and IR spectra. Structures of the complexes were further confirmed by X-ray crystallography. The molar conductance values of the complexes measured in methanol at the concentration of 10^{-3} M are in the range 4–30 $\Omega^{-1}\,cm^2\,mol^{-1}$, indicating the non-electrolytic nature of the complexes [28]. The vanadium in the complexes is +5 oxidation state and therefore EPR silent.

3.1. Structure description of the complexes

The molecular structures of the complexes **1**–**4** are shown in Figs. 1–4, respectively. X-ray crystallography reveals that the four complexes are similar centrosymmetric dimeric oxovanadium(V) compounds. The difference among the complexes is the variety of the Schiff base ligands. The V···V distances are 3.124(1) Å for **1**, 3.112(1) Å for **2**, 3.155(1) Å for **3**, and 3.170(1) Å for **4**. Each V atom in the complex is six-coordinated through three bonds to oxo groups and through three bonds to the tridentate Schiff base ligand, forming an octahedral geometry. The distances between atoms V1 and O4 in **1** and **3**, V1 and O3 in **2**, and V1 and O2 in **4** are in the range 1.608(2)–1.617(2) Å, indicating they are typical V=O bonds. The atoms O5 in **1**, O4 in **2**, O3 in **3** and **4** are bridging groups. The coordinate bond lengths in the complexes are comparable to each other, and also comparable to those observed in other similar oxovanadium complexes [29,30]. The distortion of the octahedral coordination can be observed by the coordinate bond angles, ranging from 76.3(1)° to 107.9(2)° (**1**), 76.0(1)° to 106.4(1)° (**2**), 77.0(1)° to 107.1(2)° (**3**), and 74.6(1)° to 107.0(1)° (**4**), for the perpendicular angles, and from 154.6(1)° to 170.4(1)° (**1**), 155.9(1)° to 173.3(1)° (**2**), 154.6(1)° to 171.0(1)° (**3**), 152.5(1)° to 170.3(1)° (**4**), for the diagonal angles. In each complex, there form two intramolecular N–H···O hydrogen bonds in the dimeric molecule.

Table 3
Selected bond lengths (Å) and angles (°) for the complexes.

1			
V1–O1	1.894(2)	V1–O4	1.617(3)
V1–O5	1.658(2)	V1–N1	2.134(3)
V1–N2	2.167(3)	V1–O5A	2.346(3)
O4–V1–O5	107.9(2)	O4–V1–O1	101.2(1)
O5–V1–O1	98.7(1)	O4–V1–N1	96.2(1)
O5–V1–N1	154.6(1)	O1–V1–N1	83.9(1)
O4–V1–N2	93.0(2)	O5–V1–N2	93.3(1)
O1–V1–N2	157.5(1)	N1–V1–N2	77.3(1)
O4–V1–O5A	170.4(1)	O5–V1–O5A	78.8(1)
O1–V1–O5A	84.2(1)	N1–V1–O5A	76.4(1)
N2–V1–O5A	79.6(2)		
2			
V1–O1	1.918(2)	V1–O3	1.617(2)
V1–O4	2.314(2)	V1–N1	2.164(2)
V1–N2	2.171(2)	V1–O4A	1.668(2)
O3–V1–O4A	106.4(1)	O3–V1–O1	100.7(1)
O4A–V1–O1	99.8(1)	O3–V1–N1	95.7(1)
O4A–V1–N1	155.9(1)	O1–V1–N1	84.9(1)
O3–V1–N2	94.4(1)	O4A–V1–N2	92.6(1)
O1–V1–N2	156.8(1)	N1–V1–N2	76.0(1)
O3–V1–O4	173.4(1)	O4–V1–O4A	78.4(1)
O1–V1–O4	82.8(2)	N1–V1–O4	78.8(1)
N2–V1–O4	80.6(1)		
3			
V1–O1	1.905(2)	V1–O3	2.349(2)
V1–O4	1.608(2)	V1–O3A	1.672(2)
V1–N1	2.176(3)	V1–N2	2.135(3)
O4–V1–O3A	107.1(1)	O4–V1–O1	102.2(1)
O3A–V1–O1	98.6(1)	O4–V1–N2	92.2(1)
O3A–V1–N2	92.7(1)	O1–V1–N2	158.2(1)
O4–V1–N1	96.5(1)	O3A–V1–N1	154.6(1)
O1–V1–N1	84.9(1)	N2–V1–N1	77.04(1)
O4–V1–O3	171.0(1)	O3–V1–O3A	77.94(1)
O1–V1–O3	84.1(1)	N2–V1–O3	80.0(1)
N1–V1–O3	77.5(1)		
4			
V1–O1	1.920(1)	V1–O2	1.611(2)
V1–O3	1.671(1)	V1–O3A	2.377(1)
V1–N1	2.168(2)	V1–N2	2.151(2)
O2–V1–O3	107.0(1)	O2–V1–O1	101.2(1)
O3–V1–O1	97.9(1)	O2–V1–N2	93.0(1)
O3–V1–N2	93.4(1)	O1–V1–N2	158.3(1)
O2–V1–N1	99.2(1)	O3–V1–N1	152.5(1)
O1–V1–N1	84.8(1)	N2–V1–N1	76.8(1)
O2–V1–O3A	170.3(1)	O3–V1–O3A	78.3(1)
O1–V1–O3A	85.8(1)	N2–V1–O3A	78.5(1)
N1–V1–O3A	74.6(1)		
5			
V1–O1	1.827(2)	V1–O3	1.945(2)
V1–O5	1.578(2)	V1–O6	1.744(2)
V1–N1	2.094(2)		
O5–V1–O6	109.2(1)	O5–V1–O1	105.4(1)
O6–V1–O1	99.7(1)	O5–V1–O3	102.5(1)
O6–V1–O3	88.0(1)	O1–V1–O3	146.6(1)
O5–V1–N1	99.9(1)	O6–V1–N1	148.7(1)
O1–V1–N1	83.0(1)	O3–V1–N1	74.4(1)
6			
V1–O1	1.840(3)	V1–O2	1.959(3)
V1–O4	1.578(3)	V1–O6	1.753(3)
V1–O5	2.374(3)	V1–N1	2.129(3)
O4–V1–O6	103.7(2)	O4–V1–O1	99.4(2)
O6–V1–O1	101.6(2)	O4–V1–O2	97.9(2)
O6–V1–O2	94.5(2)	O1–V1–O2	152.7(2)
O4–V1–N1	96.9(2)	O6–V1–N1	157.7(2)
O1–V1–N1	82.9(2)	O2–V1–N1	74.2(2)
O4–V1–O5	176.0(2)	O6–V1–O5	80.0(2)
O1–V1–O5	81.0(2)	O2–V1–O5	80.3(2)
N1–V1–O5	79.2(1)		

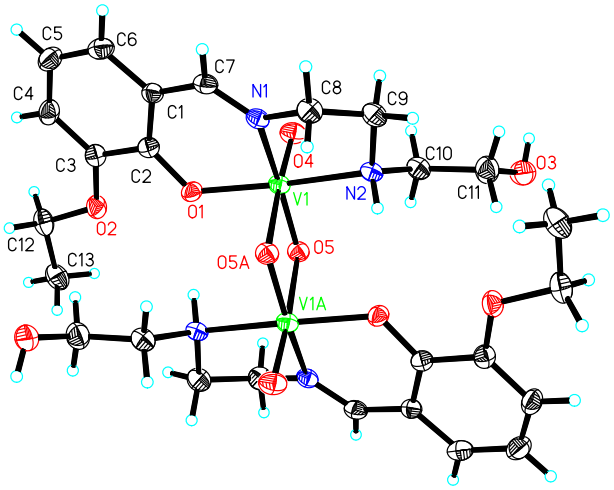

Fig. 1. A perspective view of the molecular structure of **1** with the atom labeling scheme. The thermal ellipsoids are drawn at the 30% probability level. Unlabeled atoms are related to the symmetry position $1-x, -y, 1-z$.

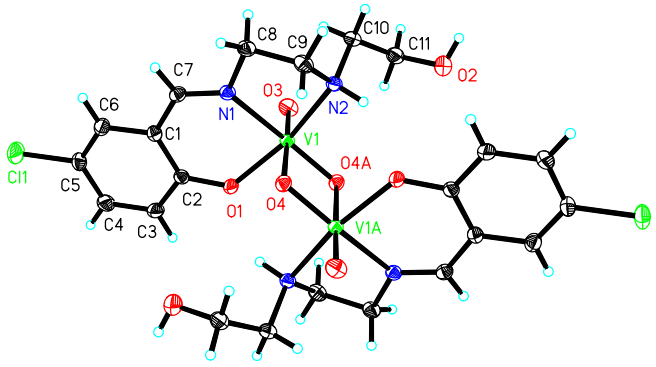

Fig. 2. A perspective view of the molecular structure of **2** with the atom labeling scheme. The thermal ellipsoids are drawn at the 30% probability level. Unlabeled atoms are related to the symmetry position $-x, 1-y, 2-z$.

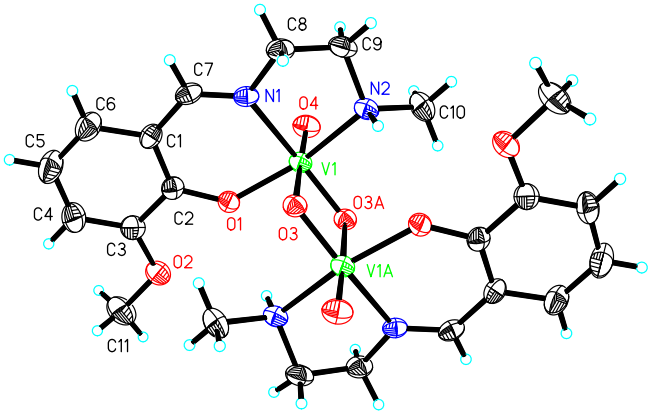

Fig. 3. A perspective view of the molecular structure of **3** with the atom labeling scheme. The thermal ellipsoids are drawn at the 30% probability level. Unlabeled atoms are related to the symmetry position $1-x, 1-y, 1-z$.

The molecular structure of the complex **5** is shown in Fig. 5. The V atom is in a distorted square-pyramidal coordination. The phenolate O, imine N, and enolic O atoms of the hydrazone ligand, and the methoxide O atom constitute the basal plane, and the oxo O atom occupies the apical position. The displacement of the V atom from the basal plane toward the apical oxo group is 0.476(1) Å. The extent of distortion of a square-pyramidal geometry toward a trigonal-bipyramidal geometry can be measured by

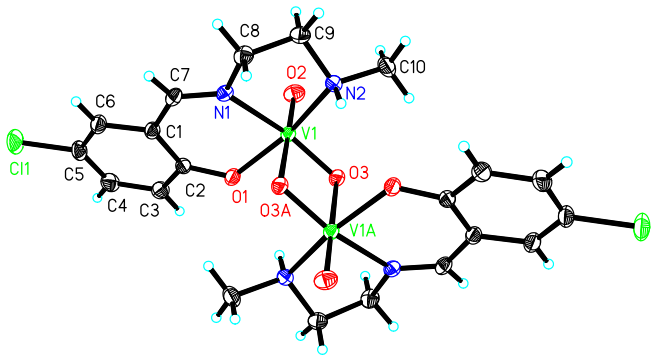

Fig. 4. A perspective view of the molecular structure of **4** with the atom labeling scheme. The thermal ellipsoids are drawn at the 30% probability level. Unlabeled atoms are related to the symmetry position $2-x, -y, -z$.

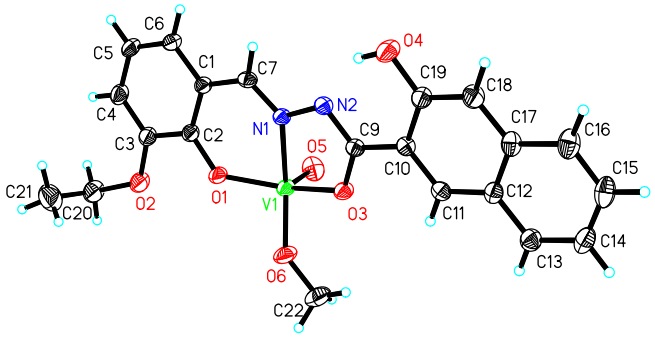

Fig. 5. A perspective view of the molecular structure of **5** with the atom labeling scheme. The thermal ellipsoids are drawn at the 30% probability level.

the value of τ which is defined as $(\beta-\alpha)/60°$, where α and β are the two larger coordinate bond angles [31]. For an ideal square-pyramidal geometry τ is 0 and for an ideal trigonal-bipyramidal geometry τ is 1. The value of τ is 0.035. Thus, the coordination can be defined as a slightly distorted octahedral geometry. The coordinate bond lengths in the complex are comparable to those observed in other similar oxovanadium complexes [32,33].

The molecular structure of complex **6** is shown in Fig. 6. The V atom in the complex is in a distorted octahedral coordination. The dianioinic tridentate ligand coordinates to the V atom through the phenolate O, imine N, and enolic O atoms, forming a six- and a five-membered chelate rings. The methoxide O atom is *trans* to the imine N atom in the molecule. The O,N,O donor atoms of the hydrazone ligand and the methoxide O atom define the equatorial plane of the octahedron. The two axial positions are occupied by one oxo O atom and one methanol O atom. The displacement of the V atom towards the O4 donor atom from the equatorial plane

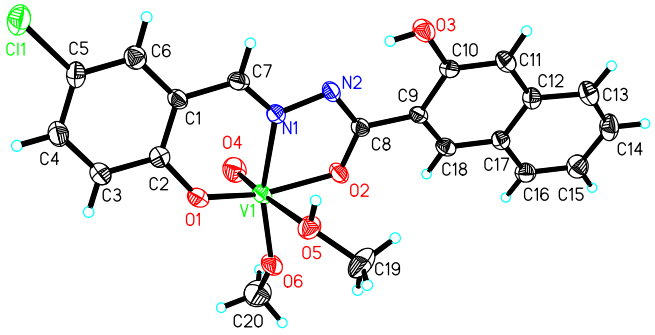

Fig. 6. A perspective view of the molecular structure of **6** with the atom labeling scheme. The thermal ellipsoids are drawn at the 30% probability level.

is 0.323(1) Å. The coordinate bond lengths in the complex are comparable to those observed in the complexes **1**–**5** and those observed in other similar complexes [33,34]. The distortion of the octahedral coordination can be observed by the coordinate bond angles, ranging from 74.2(2)° to 103.7(2)° for the perpendicular angles, and from 152.7(2)° to 176.0(2)° for the diagonal angles.

3.2. IR spectra

The IR spectra of the ligands exhibit sharp bands in the region 3200–3250 cm^{-1}, which are assigned to the ν(N–H) vibrations. The middle absorption bands in the range 3350–3470 cm^{-1} in the complexes **1**, **2**, **5**, and **6**, are assigned to the ν(O–H) vibrations. The υ(C=O) stretches in HL^5 and HL^6 and at 1653 and 1655 cm^{-1}, respectively, which are absent in the complexes **5** and **6**, consistent with the enolisation of the amide functionalities and subsequent proton replacement by the vanadium atoms. The bands appearing at 1273 and 1278 cm^{-1} for **5** and **6**, respectively, are assigned to the ν(C–O)(enolic) vibrations. The strong absorption bands at 1640 cm^{-1} in **1**, 1638 cm^{-1} in **2**, 1635 cm^{-1} in **3**, 1649 cm^{-1} in **4**, 1638 cm^{-1} in **5**, and 1641 cm^{-1} in **6**, respectively, are attributed to the ν(C=N) vibration [35]. The bands observed at 996 cm^{-1} in **1**, 970 cm^{-1} in **2**, 969 cm^{-1} in **3**, 956 cm^{-1} in **4**, 990 cm^{-1} in **5**, and 984 cm^{-1} in **6**, respectively, are assigned to the ν(V=O) stretches [34].

3.3. Pharmacology

The measurement of *H. pylori* urease inhibitory activity was carried out for three parallel times. The inhibition rates (%) with the

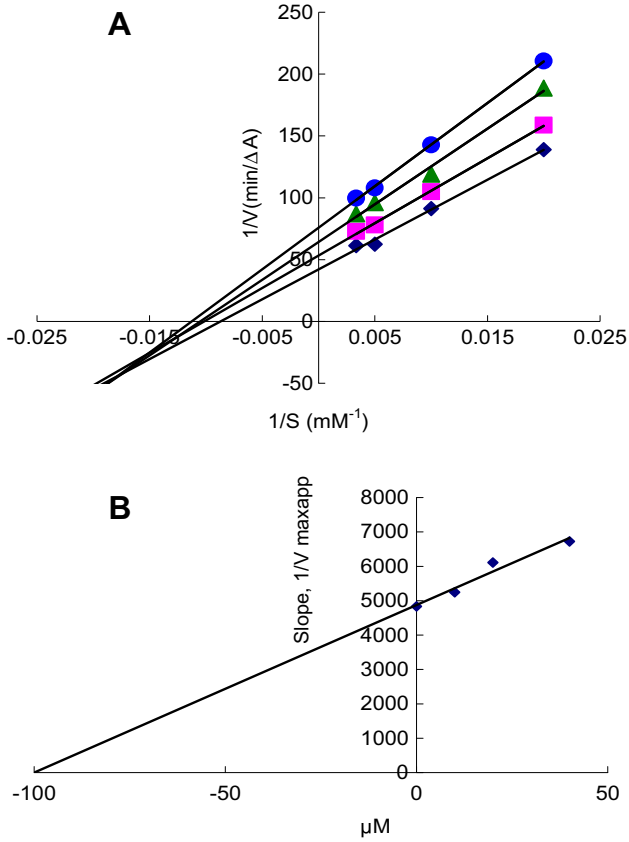

Fig. 7. Steady-state inhibiotion of urease by compound **6**. (A) Lineweaver–Burk plot of reciprocal of initial velocities vs. reciprocal of four urea concentrations in the absence (□) and presence of 10 μM (■), 20 μM (▲), and 40 μM (●) of the compound. (B) Secondary plots of the Lineweaver–Burk plot, slope vs. various concentrations of the compound.

concentration of 100 μM for the complexes are 18.96 ± 0.44 (**1**), 33.01 ± 1.80 (**2**), 35.83 ± 0.78 (**3**), 48.09 ± 1.23 (**4**), 45.91 ± 2.09 (**5**), and 90.72 ± 1.91 (**6**). The acetohydroxamic acid was used as a reference [7] with the inhibition rate (%) of 87.30 ± 3.35. It can be seen that the chloro-substituted complexes have stronger activities against urease than the methoxy- or ethoxy-substituted complexes. The trend is accord with those reported by Smee and coworkers [36]. The IC_{50} value (17.35 ± 1.01 μM) for **6** was determined since it has strong urease inhibitory activity, which is much lower than the acetohydroxamic acid (46.27 ± 0.73 μM), and also much lower than the vanadyl sulfate (207.13 ± 3.10 μM).

The Lineweaver–Burk plot (Fig. 7A) revealed that **6** is a mixed-competitive inhibitor of urease. Double plot of the Lineweaver–Burk plot (Fig. 7B) showed that the K_i value of the compound against urease was 99.99 μM.

3.4. Molecular docking study

Fig. 8 (complex **6**) is a representative of the binding model of the complexes in the enzyme active site of urease. The hydrogen bonds among the complexes and the active sites of the urease were listed in Table 4. For **1**, there is one kind of hydrogen bond formed by the hydroxy group with the O atom of *Gln*364. For **2**, there are two kinds of hydrogen bonds formed by the amino group with the O atom of *Asn*168, and by the hydroxy group with the O atom of *Asp*223. For **3** and **4**, there are no hydrogen bonds. For **5**, there is one kind of hydrogen bond formed by the hydroxyl O atom of the complex with the amino group of *Agr*338. For **6**, there are three kinds of hydrogen bonds formed by the hydroxyl O atom of the complex with the amino group of *Arg*338, by the oxo O atom of the complex with the amino group of *His*221, and by the hydroxy group of the complex with the O atom of *Asn*168. In addition, the complexes **1**, **2**, and **3** form hydrophobic interactions with *Ala*169 and *Ala*365 of the urease; the complex **4** forms hydrophobic interactions with *Leu*252 of the urease; the complexes **5** and **6** form hydrophobic interactions with *Ala*365 of the urease. It is notable that the docking score of **6** (−7.98) is lower than those of **1** (−2.79), **2** (−0.87), **3** (−0.66), **4** (−7.00), and **5** (−5.89). The result of molecular docking study could explain the strong inhibitory activity of **6** against urease.

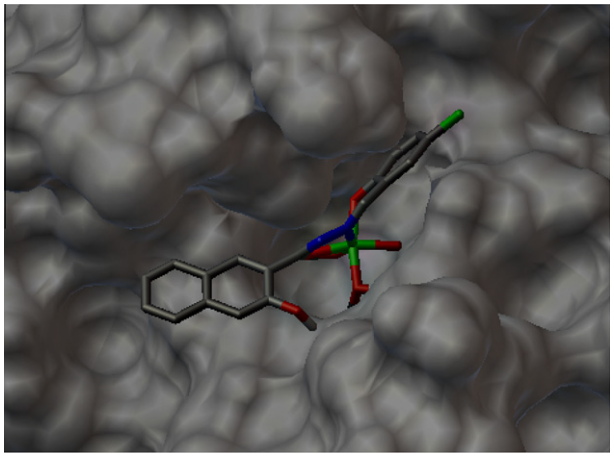

Fig. 8. Binding mode of **6** with *Helicobacter pylori* urease. The enzyme is shown as surface. The complex is shown as sticks.

Table 4
Hydrogen bonds among the complexes and the active sites of the urease.

Complex	Hydrogen bond	Length of hydrogen bond (Å)	Angle of hydrogen bond (°)
1	$O–H\cdots N_{Gln364}$	1.925	142.83
2	$N–H\cdots O_{Asn168}$	2.225	121.54
	$O–H\cdots O_{Asp223}$	2.077	149.15
5	$N–H_{Arg338}\cdots O$	2.710	125.05
6	$N–H_{Arg338}\cdots O$	2.039	169.87
	$N–H_{His221}\cdots O$	2.014	125.38
	$O–H\cdots O_{Asn168}$	1.815	155.75

4. Conclusion

This paper reports the synthesis, structures, and urease inhibitory activities of a series of oxovanadium(V) complexes with Schiff bases. The urease inhibitory activity of the complex **6** is superior to those of the acetohydroxamic acid and the other complexes. The kinetic studies reveal that the complex is a mixed-competitive inhibitor of urease. Considering the oxovanadium complexes have interesting biological activities and have been widely used in medicine [18–20,37,38], the complex **6** may be used in the treatment of infection caused by the urease producing bacteria.

Acknowledgements

This work was financially supported by the Natural Science Foundation of China (Project No. 20901036), and by the Distinguished Young Scholars Program of Higher Education of Liaoning Province (Grant No. LJQ2011114).

Appendix A. Supplementary material

CCDC 802003, 802004, 802007, 802008, 802005, and 802006 for compounds **1**–**6**, respectively, contains the supplementary crystallographic data for this paper. These data can be obtained free of charge from The Cambridge Crystallographic Data Centre via www.ccdc.cam.ac.uk/data_request/cif.

Supplementary data associated with this article can be found, in the online version, at doi:10.1016/j.ica.2011.11.039.

References

[1] P.A. Karplus, M.A. Pearson, R.P. Hausinger, Acc. Chem. Res. 30 (1997) 330.
[2] J.B. Sumner, J. Biol. Chem. 69 (1926) 435.
[3] L.E. Zonia, N.E. Stebbins, J.C. Polacco, Plant Physiol. 107 (1995) 1097.
[4] C.M. Collins, S.E.F. DÓrazio, Mol. Microbiol. 9 (1993) 907.
[5] C. Montecucco, R. Rappuoli, Nat. Rev. Mol. Cell Biol. 2 (2001) 457.
[6] W. Zhengping, O. Van Cleemput, P. Demeyer, L. Baert, Fertil. Soils 11 (1991) 41.
[7] B. Krajewska, J. Mol. Catal. B 59 (2009) 9.
[8] Z. Amtul, Atta-ur Rahman, R.A. Siddiqui, M.I. Choudhary, Curr. Med. Chem. 9 (2002) 1323.
[9] W. Zaborska, M. Kot, K. Superata, J. Enzyme Inhib. Med. Chem. 17 (2002) 247.
[10] M.A. Pearson, L.O. Michel, R.P. Hausinger, P.A. Karplus, Biochemistry 36 (1997) 8164.
[11] W. Zaborska, B. Krajewska, Z. Olech, J. Enzyme Inhib. Med. Chem. 19 (2004) 65.
[12] W. Zaborska, B. Krajewska, M. Leszko, Z. Olech, J. Mol. Catal. B 13 (2001) 103.
[13] A.Y. Louie, T.J. Meade, Chem. Rev. 99 (1999) 2711.
[14] Z.-L. You, L. Zhang, D.-H. Shi, X.-L. Wang, X.-F. Li, Y.-P. Ma, Inorg. Chem. Commun. 13 (2010) 996.
[15] Z.-L. You, L.-L. Ni, D.-H. Shi, S. Bai, Eur. J. Med. Chem. 45 (2010) 3196.
[16] P. Hou, Z.-L. You, L. Zhang, X.-L. Ma, L.-L. Ni, Transition Met. Chem. 33 (2008) 1013.
[17] M.J. Pereira, E. Carvalho, J.W. Eriksson, D.C. Crans, M. Aureliano, J. Inorg. Biochem. 103 (2009) 1687.
[18] M.-J. Xie, X.-D. Yang, W.-P. Liu, S.-P. Yan, Z.-H. Meng, J. Inorg. Biochem. 104 (2010) 851.
[19] J.J. Smee, J.A. Epps, K. Ooms, S.E. Bolte, T. Polenova, B. Baruah, L.Q. Yang, W.J. Ding, M. Li, G.R. Willsky, J. Inorg. Biochem. 103 (2009) 575.
[20] R. Ara, U. Ashiq, M. Mahroof-Tahir, Z.T. Maqsood, K.M. Khan, M.A. Lodhi, M.I. Choudhary, Chem. Biodivers. 4 (2007) 58.
[21] R. Huey, G.M. Morris, A.J. Olson, D.S. Goodsell, J. Comput. Chem. 28 (2007) 1145.
[22] Bruker, SMART (Version 5.628) and SAINT (Version 6.02), Bruker AXS Inc., Madison, Wisconsin, USA, 1998.

[23] G.M. Sheldrick, SADABS Program for Empirical Absorption Correction of Area Detector, University of Göttingen, Germany, 1996.
[24] G.M. Sheldrick, SHELXTL V5.1. Software Reference Manual, Bruker AXS, Inc., Madison, Wisconsin, USA, 1997.
[25] W.J. Mao, P.C. Lv, L. Shi, H.Q. Li, H.L. Zhu, Bioorg. Med. Chem. 17 (2009) 7531.
[26] M.W. Weatherburn, Anal. Chem. 39 (1967) 971.
[27] B. Krajewska, W. Zaborska, Bioorg. Chem. 35 (2007) 355.
[28] W.J. Geary, Coord. Chem. Rev. 7 (1971) 81.
[29] L.M. Mokry, C.J. Carrano, Inorg. Chem. 32 (1993) 6119.
[30] C.A. Root, J.D. Hoeschele, C.R. Cornman, J.W. Kampf, V.L. Pecoraro, Inorg. Chem. 32 (1993) 3855.
[31] A.W. Addison, T.N. Rao, J. Reedijk, J. van Rijn, G.C. Verschoor, J. Chem. Soc., Dalton Trans. (1984) 1349.
[32] M.S. Palacios, M.J. Rocío, S. Domínguez, P. Gili, C. Ruiz-Pérez, F.V. Rodríguez-Romero, J.-M. Dance, Polyhedron 16 (1997) 1143.
[33] A. Sarkar, S. Pal, Inorg. Chim. Acta 361 (2008) 2296.
[34] N.R. Sangeetha, V. Kavita, S. Wocadlo, A. Powell, S. Pal, J. Coord. Chem. 51 (2000) 55.
[35] S.-X. Liu, S. Gao, Inorg. Chim. Acta 282 (1998) 149.
[36] J.J. Smee, J.A. Epps, K. Ooms, S.E. Bolte, T. Polenova, B. Baruah, L. Yang, W. Ding, M. Li, G.R. Willsky, A. la Cour, O.P. Anderson, D.C. Crans, J. Inorg. Biochem. 103 (2009) 575.
[37] J.K. Jackson, W. Min, T.F. Cruz, S. Cindric, L. Arsenault, D.D. VonHoff, D. Degan, W.L. Hunter, H.M. Burt, Br. J. Cancer 75 (1997) 1014.
[38] Z.H. Chohan, S.H. Sumrra, J. Enzyme Inhib. Med. Chem. 25 (2010) 599.